

Pressure-driven superconductivity in the topological insulator GeBi_4Te_7

Yalei Huang,¹ Na Zuo,² Zheyi Zhang,¹ Chunqiang Xu,³ Xiangzhuo Xing,^{2,*} Wen-He Jiao,¹ Bin Li,^{4,†} Wei Zhou,^{5,‡} Xiaobing Liu,² Dong Qian,^{6,7,8} and Xiaofeng Xu^{1,§}

¹*School of Physics, Zhejiang University of Technology, Hangzhou 310023, China*

²*Laboratory of High Pressure Physics and Material Science (HPPMS),*

School of Physics and Physical Engineering, Qufu Normal University, Qufu 273165, China

³*School of Physical Science and Technology, Ningbo University, Ningbo 315211, China*

⁴*Information Physics Research Center, Nanjing University of Posts and Telecommunications, Nanjing 210023, China*

⁵*School of Electronic and Information Engineering,*

Changshu Institute of Technology, Changshu 215500, China

⁶*Key Laboratory of Artificial Structures and Quantum Control (Ministry of Education),*

School of Physics and Astronomy, Shanghai Jiao Tong University, Shanghai 200240, China

⁷*Tsung-Dao Lee Institute, Shanghai Jiao Tong University, Shanghai 200240, China*

⁸*Collaborative Innovation Center of Advanced Microstructures, Nanjing 210093, China*

(Dated: March 6, 2025)

The van der Waals, pseudo-binary chalcogenides $(ACh)_m(Pn_2Ch_3)_n$ ($A = \text{Ge, Mn, Pb, etc.}; Pn = \text{Sb or Bi}; Ch = \text{Te, Se}$) have recently been reported to host a vast landscape of topological phases of matter, including the quantum anomalous Hall state and topological axion state with quantized magnetoelectric effect. A subgroup in this series, like MnSb_4Te_7 and GeSb_4Te_7 , can be driven to a superconducting state by applying a physical pressure, making them viable candidates to realize so-called topological superconductivity. However, the role of magnetic fluctuations in this pressure-induced superconductivity remains unclear. Here, we report the pressure-induced multiple superconducting phases in the nonmagnetic GeBi_4Te_7 , accompanied by corresponding structural transitions evidenced from the high-pressure Raman scattering. In comparison with other members in this family, we find the superconducting transition temperature of the nonmagnetic subgroup is significantly higher than their magnetic homologues, possibly hinting at the detrimental role played by the magnetic fluctuations in the superconductivity formation, at least in this pseudo-binary chalcogenide family.

Engineering superconductivity in topological materials is generally believed to be an effective approach to achieving topological superconductivity with emergent Majorana fermions, the manipulation of which lays the foundation for future applications in fault-tolerant topological quantum computing¹⁻⁴. Among the various means of tuning, such as chemical substitution or intercalation, pressure proves to be a clean and fruitful way in the quest for topological superconductor candidates. Indeed, superconductivity achieved in this manner has been observed in some archetypal topological insulator (TI) candidates. For example, TIs Bi_2Se_3 and Sb_2Te_3 become bulk superconductors by the application of pressure, with a maximum T_c value of 7 K and 6.3 K, respectively^{5,6}.

Among a large number of as yet discovered topological materials, the multilayered, pseudo-binary chalcogenides $(ACh)_m(Pn_2Ch_3)_n$ ($A = \text{Ge, Mn, Pb, etc.}; Pn = \text{Sb or Bi}; Ch = \text{Te, Se}$) are of particular interest⁷⁻¹¹. On one hand, Pn_2Ch_3 , i.e., $m=0, n=1$, were the first validated bulk TIs, thereafter opening the door to search for versatile topological properties of hundreds of other materials. Structurally, these Bi_2Te_3 -type compounds crystallize in the tetradymite-like layered structure, consisting of Te-Bi-Te-Bi-Te quintuple layers (5L,QLs) that are stacked along the c -axis by van der Waals forces (see Fig. 1(a) for the structural motif)¹². On the other hand, the ACh bilayer can readily intercalate the QLs, forming the Ch - Pn - Ch - A - Ch - Pn - Ch septuple layers (7L,SLs) (Fig. 1(b)). With these QLs and SLs as the basic building elements, new van der Waals compounds $(ACh)_m(Pn_2Ch_3)_n$ can be formed. For concreteness, in the 124 phase, i.e., $m=1, n=1$, the structure is established by the stacking of SLs only (Fig. 1(b)), whereas in the 147 phase, i.e., $m=1, n=2$, it consists of alternating stacking of QLs and SLs along the c -axis, forming a natural superlattice (Fig. 1(c)). Re-

markably, most members in this family were reported to be 3D TIs, offering a tunable platform to observe diverse topological phenomena, including topological superconductivity.

In the past few years, substantial research efforts have been devoted to tuning the superconductivity in these pseudo-binary chalcogenides $(ACh)_m(Pn_2Ch_3)_n$ ^{8,9,13,14}. For instance, besides the above mentioned Bi_2Se_3 and Sb_2Te_3 , superconductivity was reported in SnSb_2Te_4 under pressure where T_c is gradually enhanced with increasing pressure up to 33 GPa¹⁵. Superconductivity was later revealed in both crystalline and amorphous forms of GeSb_2Te_4 , with two superconducting phases being observed for $P < 40$ GPa^{13,14}. More recently, superconductivity was also found in the pressurized GeSb_4Te_7 ⁸.

Surprisingly though, superconductivity was not observed in the pressurized magnetic MnBi_2Te_4 and MnBi_4Te_7 ¹⁰. Intriguingly, MnSb_4Te_7 was recently reported to show a dome-like phase diagram with a maximum T_c of only 2.2 K at ~ 50 GPa⁹, significantly lower than its nonmagnetic sibling GeSb_4Te_7 which has a maximum T_c of approximate 8 K at 35 GPa⁸, leading to the conjecture that the magnetic fluctuations in the Mn-based homologues may be adverse to the formation of Cooper pairs.

In this study, we report the pressure-induced multiple superconducting phases in GeBi_4Te_7 . To be specific, we observed three superconducting phases between 8 GPa and 42 GPa, with the maximum T_c over 8 K at ~ 30 GPa. These three superconducting phases are driven by the putative structural phase transitions, in analogy to what was observed in GeSb_4Te_7 ⁸. By comparing with other members in this class of materials, in particular the magnetic MnBi_4Te_7 ¹⁰, our study suggests that the magnetic fluctuations play a possible unfavorable role in

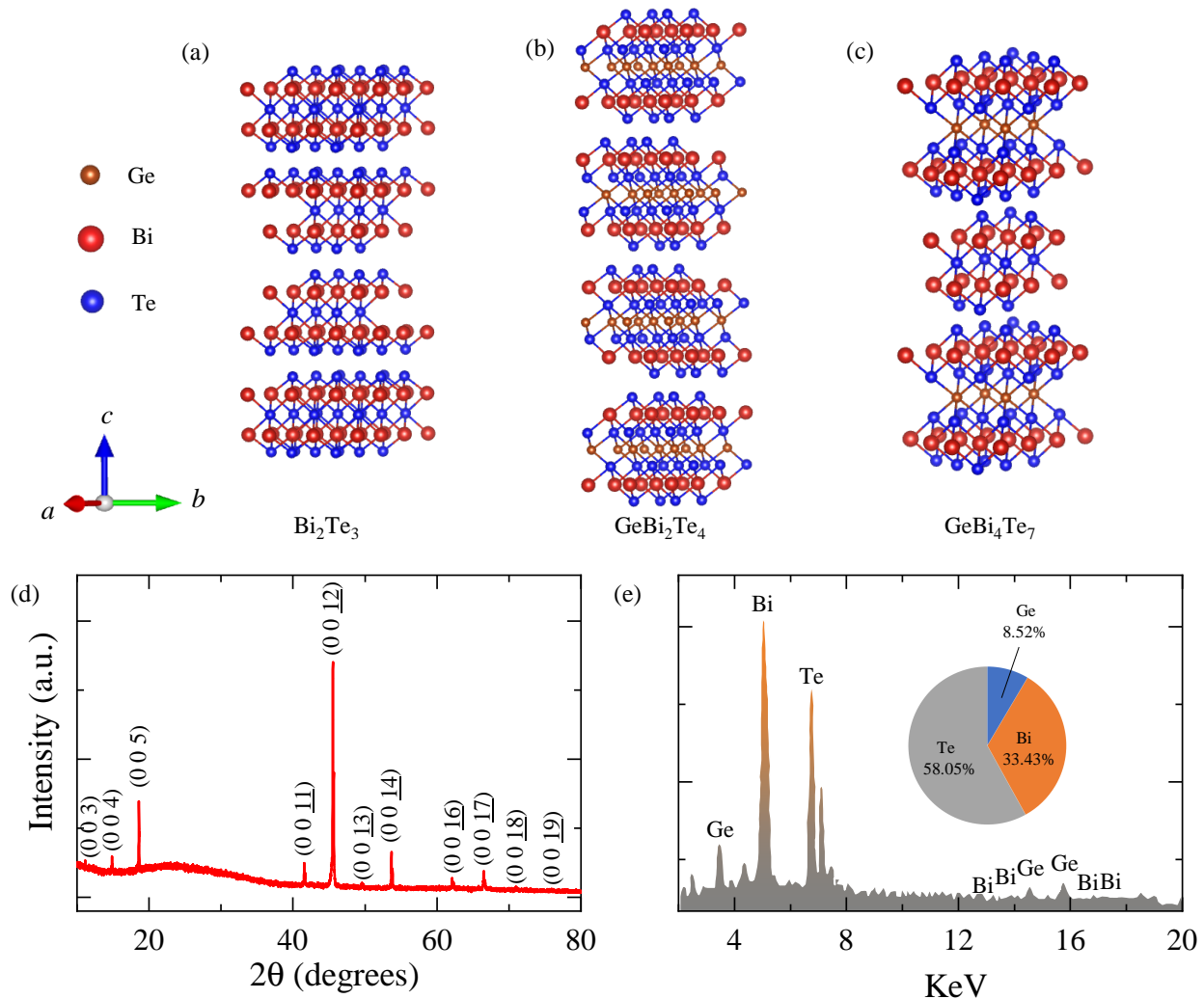


FIG. 1: (a)-(c) The crystal structure of the pseudo-binary chalcogenides $(ACh)_m(Pn_2Ch_3)_n$, represented by $A=\text{Ge}$, $Pn=\text{Bi}$, $Ch=\text{Te}$. In panel (a), $m=0$, $n=1$. In panel (b), $m=1$, $n=1$. In panel (c), $m=1$, $n=2$. (d) The single crystal XRD of the GeBi_4Te_7 sample. Only $(00l)$ peaks have been observed, indicating the sample top facet is along the c axis. (e) A typical EDX pattern showing the stoichiometric ratio of Ge:Bi:Te is very close to 1:4:7.

the superconductivity formation, at least in these pseudo-binary chalcogenide systems.

Single crystals of GeBi_4Te_7 were synthesized by the self-flux method¹⁶. The elements of Ge, Bi and Te were mixed in a molar ratio of 1:4:15, placed into an alumina crucible, and sealed in an evacuated quartz tube. Subsequently, the mixture was heated to 1050 °C over a period of 12 hours, then slowly cooled down to 500 °C at a rate of 2 °C per hour, followed by centrifugation to remove the excess flux. The van der Waals crystals of GeBi_4Te_7 , with a typical size of $2\times 2\times 0.1\text{ mm}^3$, were achieved. The composition of the single crystals was determined by the energy-dispersive x-ray spectroscopy (EDS) on a scanning electron microscope (Hitachi S-3700N) equipped with an Oxford Instruments X-Max spectrometer. X-ray diffraction (XRD) was carried out on a PANalytical x-ray diffractometer (Model EMPYREAN) with monochromatic Cu $K\alpha$ radiation at room temperature. The electrical transport properties were measured in a cryostat from Cryogenic Instruments using a standard four-probe method. The MR and Hall resistivity were measured by changing the polarities of the field and symmetrizing and anti-symmetrizing the data, respectively. High-pressure transport experiments

were conducted in a nonmagnetic Be-Cu diamond anvil cell with NaCl as the pressure transmitting medium. A single crystal with dimensions of $130\times 50\times 10\ \mu\text{m}^3$ was loaded together with some ruby powder. High-pressure Raman spectroscopy data were collected by a Renishaw inVia Raman system with a laser wavelength of 532 nm.

The electronic structure of GeBi_4Te_7 was investigated using first-principles density functional theory (DFT) calculations implemented within the WIEN2K package¹⁷, employing the full-potential linearized augmented plane wave (FLAPW) method. We utilized the Wu-Cohen generalized gradient approximation (GGA)¹⁸ for the exchange-correlation functional, with $18\times 18\times 2$ k -point mesh in the self-consistent field calculation. To ensure a comprehensive and accurate description of the electronic structure, the spin-orbit coupling (SOC) were incorporated in all calculations. The Fermi surface was mapped using a high-density $40\times 40\times 7$ k -point mesh across the complete Brillouin zone (BZ). We checked the topological properties using the Elementary Band Representations (EBRs) method^{19,20}. At each maximal k -vector, we first determined the collection of irreducible representations. Subsequently, by applying compatibility relations and ref-

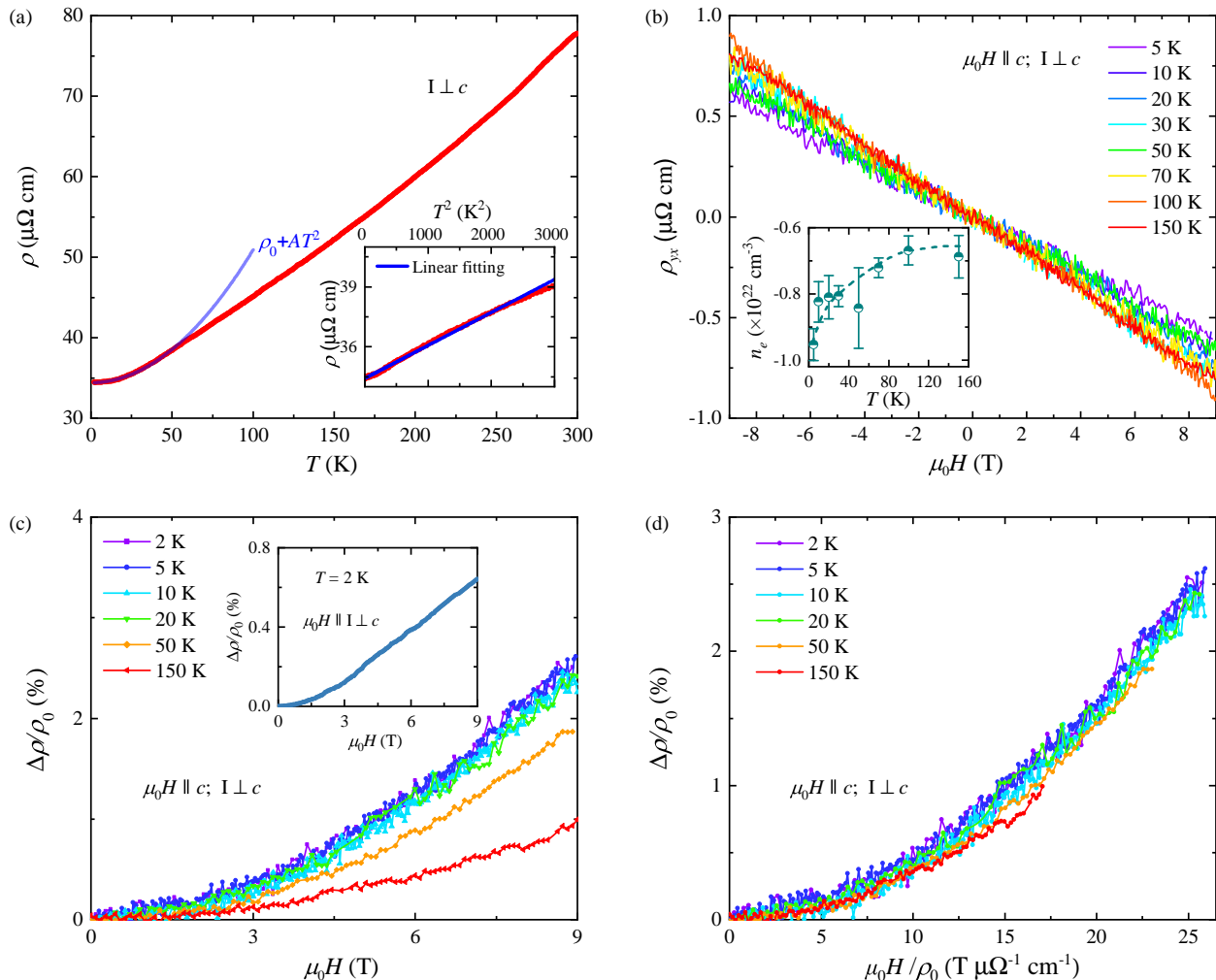


FIG. 2: (a) The zero-field in-plane resistivity. Below ~ 50 K, a Fermi liquid behavior is seen which is better resolved in the inset when plotted as ρ vs T^2 . (b) The Hall resistivity ρ_{yx} at some fixed temperatures showing quasi-linear scaling with field. The inset shows the electron density n_e extracted from the single-band fitting. (c) The TMR at some fixed temperatures. The inset shows the longitudinal magnetoresistance at 2 K as a comparison. (d) The Kohler's plot of the data in panel (c).

erencing the EBRs, we verified whether the band structure can be decomposed into linear combinations of EBRs with integer coefficients. We also constructed a tight-binding model using maximally localized Wannier functions (MLWFs)²¹ as implemented in the Wannier Tools package²². The tight-binding Hamiltonian was built using 72 bands, incorporating Ge 4*p*, Bi 6*p* and Te 5*p* orbitals as the basis for the topological analysis.

The single crystal XRD pattern at ambient conditions has been demonstrated in Fig. 1(d). All peaks can be well indexed by the (00*l*) reflections of the trigonal $P\bar{3}m1$ (No. 164) space group, indicating the crystallographic *c*-axis is normal to the sample top facet. The calculated *c*-axis lattice constant is $c=23.90$ Å, in excellent agreement with the published value¹⁶. The chemical composition of the single crystals was checked by the EDS with a typical spectrum given in Fig. 1(e). The stoichiometry of the constituent Ge, Bi and Te was seen to be very close to 1:4:7 from the multiple-spot scanning on the surface, confirming the high quality of the GeBi₄Te₇ single crystals used in this study.

The in-plane resistivity ($I\parallel ab$) has been measured from room temperature down to 2 K (Fig. 2(a)). The metallic

$\rho(T)$ profile is seen, with the residual resistivity ratio (RRR) of ~ 2 , indicating the poor metallicity. Below ~ 50 K, resistivity follows a T^2 behavior, indicating a Fermi liquid ground state²³. This T^2 scaling is better visualized in the inset of Fig. 2(a). The Hall resistivity ρ_{yx} has been measured at some fixed temperatures between 5 K and 150 K, as shown in Fig. 2(b). It is seen that ρ_{yx} has a negative slope and is quasi-linear in field, suggesting the dominant electron-type carriers. The carrier density n_e can be extracted from $n_e = \frac{1}{eR_H}$, where $R_H = \frac{\rho_{yx}}{B}$. The carrier density n_e , as a function of temperature, is displayed in Fig. 2(b) inset. With decreasing temperature, n_e increases slightly.

The transverse magnetoresistance (TMR), with the current applied along the *ab* plane and the magnetic field along the *c*-axis, has been measured, as plotted in Fig. 2(c). As noted, the TMR is quadratic in field and its magnitude is rather small, with $\Delta\rho/\rho_0$ of only 2.6% at 2 K and 9 T. The longitudinal magnetoresistance is a factor of 4 smaller, as shown in the inset of Fig. 2(c). The Kohler's scaling, plotted as $\Delta\rho/\rho_0$ as a function of $\mu_0 H/\rho_0$ at different temperatures as shown in Fig. 2(d), is well obeyed in the measured temperature range, suggesting

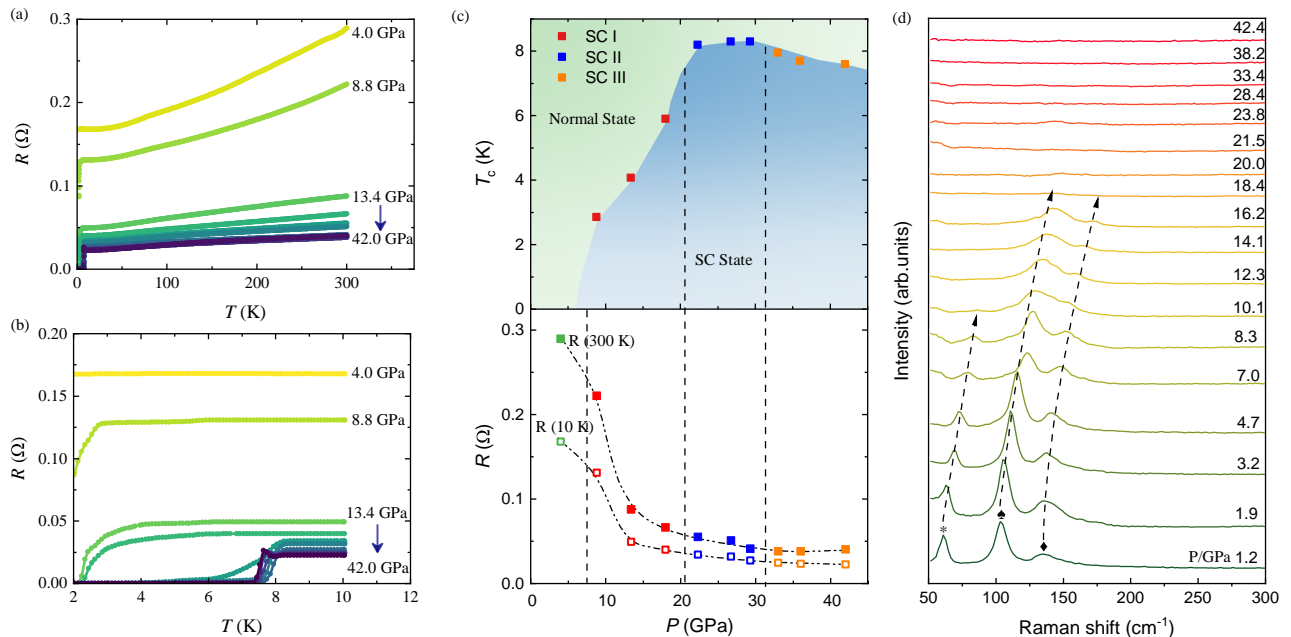


FIG. 3: (a) The resistance down to 2 K at various pressures. (b) The zoomed-in view of the low-temperature resistance. (c) The pressure phase diagram (top) and the resistances at 300 K and 10 K (bottom). (d) The pressure evolution of the Raman spectra at different pressures.

no exotic electron scattering or phase transitions^{24,25}. It is intriguing to examine the Kohler's rule in the magnetic analogues, such as MnBi_2Te_4 and MnBi_4Te_7 . However, there is no such reports in the literature thus far.

We now turn to the pressure effects on the transport properties of GeBi_4Te_7 . As shown in Fig. 3(a), $R(T)$ curves have been measured under pressures up to 42 GPa. The pressure is seen to overall suppress the resistance in the whole temperature range. The low- T region, as enlarged in Fig. 3(b), signifies the pressure-induced superconductivity. Specifically, at ~ 8.8 GPa, superconductivity starts to set in below ~ 2.8 K. Further increase of pressure boosts T_c to above 8 K when $P > 22$ GPa. Above 30 GPa, however, T_c begins to decrease with increasing pressure. The resultant phase diagram is illustrated in Fig. 3(c), highlighting the pressure-induced superconducting phase in this multilayered pseudo-binary chalcogenide GeBi_4Te_7 . The resistances at 300 K and at 10 K, are extracted in Fig. 3(c) as a function of pressure. Reminiscent of GeSb_4Te_7 ⁸, four regions are tentatively compartmentalized based on the pressure dependent T_c and $R(300\text{ K})$ and $R(10\text{ K})$ (see Fig. 3(c)).

To have more insights on the possible pressure-induced structural transitions in GeBi_4Te_7 , we performed the Raman scattering measurements under pressure, as shown in Fig. 3(d). At 1.2 GPa, there are three Raman modes at 62 cm^{-1} , 103 cm^{-1} and 135 cm^{-1} , respectively. With increasing pressure, these modes shift to higher wave numbers. Above 8.3 GPa, the first Raman peak becomes unresolvable while the other two remain to move to higher wave numbers with increasing pressure, possibly indicating a structural transition. Above 20 GPa, no peaks can be observed, indicating another possible structural transition or pressure-induced amorphization.

Figure 4 shows that with spin-orbit coupling, the electronic band structure exhibits two splitting bands crossing the Fermi level. The three-dimensional and top view of the Fermi surface reveals six-fold symmetry, consisting of one electron pocket at the BZ center and six groups of multi-component hole pockets distributed around the BZ. We analyzed the topological properties of GeBi_4Te_7 using topological indices calculated from the EBRs method. The set of bands below the Fermi level cannot be expressed as a linear combination of EBRs alone but can be represented as a linear combination of EBRs and disconnected parts of EBRs. Our analysis identifies the compound to be a topological insulator with topological indices $z_{2w,3}=1$ and $z_4=1$.

Before closing, let us compare the high-pressure phase diagram of GeBi_4Te_7 extracted from this study, with those of other members in this class of pseudo-binary chalcogenides whose pressure effects have been investigated in the literature. The most direct comparison is with the isostructural MnBi_4Te_7 that has an antiferromagnetic ground state¹⁰. Pressure changes dramatically the resistivity of MnBi_4Te_7 and induces a non-monotonic evolution of $\rho(T)$ due to two high-pressure phase transitions¹⁰. However, no superconductivity is observed up to ~ 50 GPa. Applying pressure on MnBi_2Te_4 induces metal-semiconductor-metal transitions with possible structural transitions and the concomitant changes in the topological properties¹⁰. Again, no superconductivity develops up to ~ 50 GPa. Pressure-induced superconductivity was not reported in the magnetic subgroup of this pseudo-binary chalcogenide family until the very recent observation of superconductivity under pressure in the magnetic MnSb_4Te_7 ⁹. Compared with MnBi_2Te_4 and MnBi_4Te_7 , however, the magnetic interaction seems to be weaker in

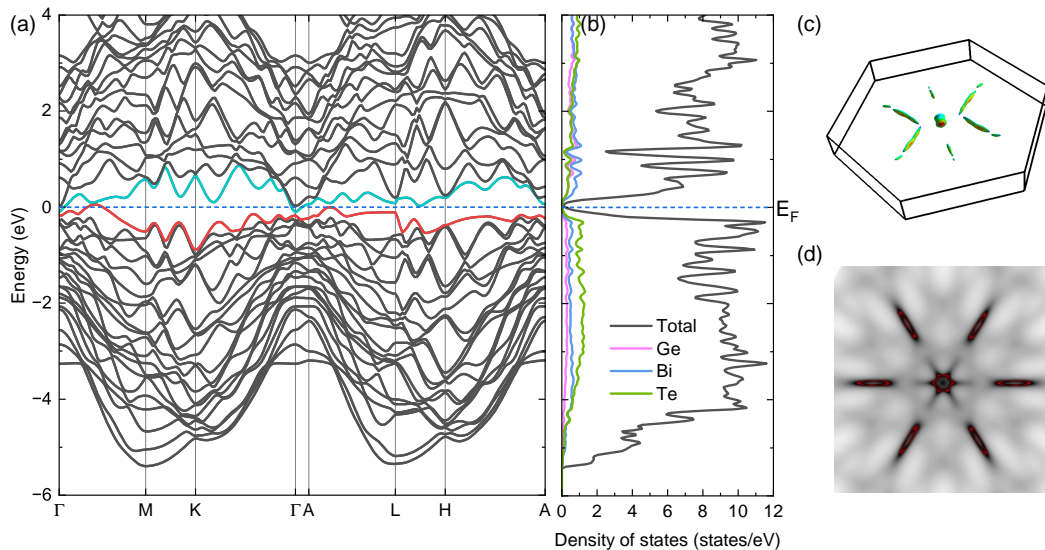


FIG. 4: Electronic properties of GeBi_4Te_7 : (a) Band structure along the high-symmetry path Γ -X-M- Γ -A-L-H-A in the Brillouin zone, highlighting the two bands (colored) that cross the Fermi level. (b) Total and partial density of states (DOS). (c) Three-dimensional visualization of the Fermi surfaces with color mapping representing the Fermi velocity. (d) Top view of the Fermi surfaces obtained from Wannier function calculations, illustrating the six-fold symmetry.

TABLE I: The pressure-induced superconductivity in the pseudo-binary chalcogenides $(ACh)_m(Pn_2Ch_3)_n$ ($A = \text{Ge, Mn, Pb}$, etc.; $Pn = \text{Sb or Bi}$; $Ch = \text{Te, Se}$). Here ‘ \times ’ denotes that no superconductivity is observed under pressure. ‘?’ means no report on the pressure study in the literature. T_c here indicates the maximum T_c in the pressure range studied, i.e., usually up to ≥ 50 GPa.

magnetic	SC under pressure	nonmagnetic	SC under pressure
MnBi_2Te_4	\times^{10}	GeBi_2Te_4	$T_c \sim 8$ K ²⁶
MnBi_4Te_7	\times^{10}	GeBi_4Te_7	$T_c \sim 8.3$ K [this work]
MnSb_2Te_4	\times^{27}	GeSb_2Te_4	$T_c \sim 7$ K ^{13,14}
MnSb_4Te_7	$T_c \sim 2$ K ⁹	GeSb_4Te_7	$T_c \sim 8$ K ⁸
$\text{MnBi}_6\text{Te}_{10}$	\times^{28}	SnSb_2Te_4	$T_c \sim 7.4$ K ¹⁵
$\text{MnSb}_6\text{Te}_{10}$?	Bi_2Te_3	$T_c \sim 8$ K ²⁹
		Sb_2Te_3	$T_c \sim 6.3$ K ⁶
		Bi_2Se_3	$T_c \sim 7$ K ⁵

MnSb_4Te_7 ⁹. Moreover, compared with the nonmagnetic GeSb_4Te_7 , superconducting T_c is much lower in the magnetic MnSb_4Te_7 ; superconducting T_c was observed when $P > 30$ GPa, reaching a maximum T_c of 2 K at 50 GPa in MnSb_4Te_7 while in GeSb_4Te_7 , T_c sets in above 10 GPa and continues to rise with increasing pressure with no sign of saturation up to ~ 35 GPa^{8,9}. By the same token, the nonmagnetic GeBi_2Te_4 has a T_c over 8 K at the pressure of ~ 15 GPa²⁶, while no superconductivity was reported for the pressurized MnBi_2Te_4 ¹⁰. These observations do seem to suggest that magnetic fluctuations play an adverse role in the superconductivity formation, at least in this class of materials. This argument is further buttressed up by the reported superconductivity in GeSb_2Te_4 under pressure ($T_c = 7$ K at $P = 20$ GPa) that is nonmagnetic

in origin^{13,14}. Table I compares the pressure effects on superconductivity in the the magnetic and nonmagnetic pseudo-binary chalcogenides that have been studied thus far.

In summary, we have successfully grown the single crystals of the layered van der Waals pseudo-binary chalcogenide GeBi_4Te_7 . We revealed the (multiple) superconducting phases under pressures up to 42 GPa. Its topological properties have also been analyzed by the first-principles calculations. By comparing with the pressure effects in other members of this class of pseudo-binary chalcogenides, our study suggests that the magnetic fluctuations may be unfavorable to the formation of superconductivity in this family of topological materials.

* Electronic address: xzxing@qfnu.edu.cn

† Electronic address: libin@njupt.edu.cn

‡ Electronic address: wei.zhou@cslg.edu.cn

§ Electronic address: xuxiaofeng@zjut.edu.cn

¹ M. Z. Hasan and C. L. Kane, Colloquium: Topological insulators, *Rev. Mod. Phys.* **82**, 3045 (2010).

² C. Nayak, S. H. Simon, A. Stern, M. Freedman, and S. D. Sarma, Non-abelian anyons and topological quantum computation, *Rev. Mod. Phys.* **80**, 1083 (2008).

³ N. P. Armitage, E. J. Mele, and A. Vishwanath, Weyl and Dirac semimetals in three-dimensional solids, *Rev. Mod. Phys.* **90**, 015001 (2018).

- ⁴ B. Yan and S.-C. Zhang, Topological materials, *Rep. Prog. Phys.* **75**, 096501 (2012).
- ⁵ K. Kirshenbaum, P. S. Syers, A. P. Hope, N. P. Butch, J. R. Jeffries, S. T. Weir, J. J. Hamlin, M. B. Maple, Y. K. Vohra, and J. Paglione, Pressure-induced unconventional superconducting phase in the topological insulator Bi_2Se_3 , *Phys. Rev. Lett.* **111**, 087001 (2013).
- ⁶ J. Zhu, J. L. Zhang, P. P. Kong, S. J. Zhang, X. H. Yu, J. L. Zhu, Q. Q. Liu, X. Li, R. C. Yu, R. Ahuja, W. Yang, G. Y. Shen, H. K. Mao, H. Weng, X. Dai, Z. Fang, Y. S. Zhao, and C. Jin, Superconductivity in topological insulator Sb_2Te_3 induced by pressure, *Sci. Rep.* **3**, 2016 (2013).
- ⁷ S. Muff, F. von Rohr, G. Landolt, B. Slomski, A. Schilling, R. J. Cava, J. Osterwalder, and J. H. Dil, Separating the bulk and surface n - to p -type transition in the topological insulator $\text{GeBi}_{4-x}\text{Sb}_x\text{Te}_7$, *Phys. Rev. B* **88**, 035407 (2013).
- ⁸ W. Zhou, B. Li, Y. Shen, J. J. Feng, C. Q. Xu, H. T. Guo, Z. He, B. Qian, Z. Zhu, and X. Xu, Multiple superconducting phases driven by pressure in the topological insulator GeSb_4Te_7 , *Phys. Rev. B* **108**, 184504 (2023).
- ⁹ C. Pei, M. Xi, Q. Wang, W. Shi, J. Wu, L. Gao, Y. Zhao, S. Tian, W. Cao, C. Li, M. Zhang, S. Zhu, Y. Chen, H. Lei, and Y. Qi, Pressure-induced superconductivity in magnetic topological insulator candidate MnSb_4Te_7 , *Phys. Rev. Mater.* **6**, L101801 (2022).
- ¹⁰ C. Pei, Y. Xia, J. Wu, Y. Zhao, L. Gao, T. Ying, B. Gao, N. Li, W. Yang, D. Zhang, H. Gou, Y. Chen, H. Hosono, G. Li, and Y. Qi, Pressure-induced topological and structural phase transitions in an antiferromagnetic topological insulator, *Chin. Phys. Lett.* **37**, 066401 (2020).
- ¹¹ S. Huan, S. Zhang, Z. Jiang, H. Su, H. Wang, X. Zhang, Y. Yang, Z. Liu, X. Wang, N. Yu, Z. Zou, D. Shen, J. Liu, and Y. Guo, Multiple magnetic topological phases in bulk van der waals crystal MnSb_4Te_7 , *Phys. Rev. Lett.* **126**, 246601 (2021).
- ¹² S. V. Eremeev, G. Landolt, T. V. Menshchikova, B. Slomski, Y. M. Koroteev, Z. S. Aliev, M. B. Babanly, J. Henk, A. Ernst, L. Patthey, A. Eich, A. A. Khajetoorians, J. Hagemeyer, O. Pietzsch, J. Wiebe, R. Wiesendanger, P. M. Echenique, S. S. Tsirkin, I. R. Amiraslanov, J. H. Dil, and E. V. Chulkov, Atom-specific spin mapping and buried topological states in a homologous series of topological insulators, *Nat. Commun.* **3**, 635 (2012).
- ¹³ E. Greenberg, B. Hen, S. Layek, I. Pozin, R. Friedman, V. Shelukhin, Y. Rosenberg, M. Karpovski, M. P. Pasternak, E. Sterer, Y. Dagan, G. K. Rozenberg, and A. Palevski, Superconductivity in multiple phases of compressed GeSb_2Te_4 , *Phys. Rev. B* **95**, 064514 (2017).
- ¹⁴ B. Hen, S. Layek, M. Goldstein, V. Shelukhin, M. Shulman, M. Karpovski, E. Greenberg, E. Sterer, Y. Dagan, G. K. Rozenberg, and A. Palevski, Superconductor-insulator transition in fcc GeSb_2Te_4 at elevated pressures, *Phys. Rev. B* **97**, 024513 (2018).
- ¹⁵ P. Song, R. Matsumoto, Z. Hou, S. Adachi, H. Hara, Y. Saito, P. B. Castro, H. Takeya, and Y. Takano, Pressure-induced superconductivity in SnSb_2Te_4 , *J. Phys.: Condens. Matter* **32**, 235901 (2020).
- ¹⁶ F. von Rohr, A. Schilling, and R. J. Cava, Single-crystal growth and thermoelectric properties of $\text{Ge}(\text{Bi,Sb})_4\text{Te}_7$, *J. Phys.: Condens. Matter* **25**, 075804 (2013).
- ¹⁷ K. Schwarz, P. Blaha, and G. K. H. Madsen, Electronic structure calculations of solids using the WIEN2k package for material sciences, *Comput. Phys. Commun.* **71**, 147 (2002).
- ¹⁸ Z. Wu and R. E. Cohen, More accurate generalized gradient approximation for solids, *Phys. Rev. B* **73**, 235116 (2006).
- ¹⁹ M. G. Vergniory, L. Elcoro, C. Felser, N. Regnault, B. A. Bernevig, and Z. Wang, A complete catalogue of high-quality topological materials, *Nature* **566**, 480 (2019).
- ²⁰ M. G. Vergniory, B. J. Wieder, L. Elcoro, S. S. P. Parkin, C. Felser, B. A. Bernevig, and N. Regnault, All topological bands of all nonmagnetic stoichiometric materials, *Science* **376**, eabg9094 (2022).
- ²¹ A. A. Mostofi, J. R. Yates, G. Pizzi, Y. S. Lee, I. Souza, D. Vanderbilt, and N. Marzari, An updated version of wannier90: A tool for obtaining maximally-localised wannier functions, *Comput. Phys. Commun.* **185**, 2309 (2014).
- ²² Q. S. Wu, S. N. Zhang, H. F. Song, M. Troyer, and A. A. Soluyanov, Wanniertools: An open-source software package for novel topological materials, *Comput. Phys. Commun.* **224**, 405 (2018).
- ²³ X. Xu, *Thermal and electrical transport in quasi-one-dimensional oxides*, PhD thesis (Univeristy of Bristol, UK, 2009).
- ²⁴ J. Xu, F. Han, T. Wang, L. R. Thoutam, S. E. Pate, M. Li, X. Zhang, Y. Wang, R. Fotovat, U. Welp, X. Zhou, W.-K. Kwok, D. Chung, M. G. Kanatzidis, and Z.-L. Xiao, Extended Kohler's rule of magnetoresistance, *Phys. Rev. X* **11**, 041029 (2021).
- ²⁵ P. Chudzinski, M. Berben, X. Xu, N. Wakeham, B. Bernáth, C. Duffy, R. D. H. Hinlopen, Y.-T. Hsu, S. Wiedmann, P. Tinnemans, R. Jin, M. Greenblatt, and N. E. Hussey, Emergent symmetry in a low-dimensional superconductor on the edge of mottness, *Science* **382**, 792 (2023).
- ²⁶ C. Liu, Y. Gao, C. Tian, C. Jiang, C. Zhu, X. Wu, X. Huang, and T. Cui, Pressure-driven dome-shaped superconductivity in topological insulator GeBi_2Te_4 , *J. Phys.: Condens. Matter* **36**, 225703 (2024).
- ²⁷ Y. Yin, X. Ma, D. Yan, C. Yi, B. Yue, J. Dai, L. Zhao, X. Yu, Y. G. Shi, J. Wang, and F. Hong, Pressure-driven electronic and structural phase transition in intrinsic magnetic topological insulator MnSb_2Te_4 , *Phys. Rev. B* **104**, 174114 (2021).
- ²⁸ J. Shao, Y. Liu, M. Zeng, J. Li, X. Wu, X. Ma, F. Jin, R. Lu, Y. Sun, M. Gu, K. Wang, W. Wu, L. Wu, C. Liu, Q. Liu, and Y. Zhao, Pressure-tuned intralayer exchange in superlattice-like $\text{MnBi}_2\text{Te}_4/(\text{Bi}_2\text{Te}_3)_n$ topological insulators, *Nano Lett.* **21**, 5874 (2021).
- ²⁹ J. L. Zhang, S. J. Zhang, H. M. Weng, W. Zhang, L. X. Yang, Q. Q. Liu, S. M. Feng, X. C. Wang, R. C. Yu, L. Z. Cao, L. Wang, W. G. Yang, H. Z. Liu, W. Y. Zhao, S. C. Zhang, X. Dai, Z. Fang, and C. Q. Jin, Pressure-induced superconductivity in topological parent compound Bi_2Te_3 , *Proc. Natl. Acad. Sci.* **108**, 24 (2011).